Full-vectorial time-domain modelling of photonic crystal semiconductor lasers

Wolfram H.P. Pernice (1), Dominic F.G. Gallagher (2) and Frank P. Payne (1)
1) Oxford University, Department of Engineering Science, Parks Road,Oxford, OX1 3PJ, UK,
wolfram.pernice@eng.ox.ac.uk
2) Photon Design, 34 Leopold Street, Oxford, OX4 1TW, UK

Abstract: *We present a novel numerical scheme for the simulation of photonic crystal lasers with nonlinear response. The gain of the lasing material is closely modelled over a large wavelength range. High computational efficiency is achieved by using refined meshes and implementing the method for distributed computing.*

Introduction

Photonic crystals show promise for shaping the optical properties of semiconductor lasers. They are for example used to optimise beam quality of VCSEL lasers [1] and to achieve low-threshold [2] or ultrafast lasers [3]. However, the design of such structures provides serious challenges to numerical methods available to date. For one, the material properties of the lasing material have to be described accordingly in the algorithm. In addition, the structural size of the device under consideration often overextends the computational hardware available in standard research facilities.

We present an efficient numerical solution to these challenges. We use the finite-difference time-domain (FDTD) method [4] due to its flexibility to handle complex geometric and material systems. Material gain is included into the standard FDTD algorithm by linking the gain to a frequency dependent conductivity. Because data for material gain in a quantum well structure is readily available [5], we choose to incorporate active material behaviour using the conductivity, which can be expressed in terms of the material gain and therefore allows us to describe complex vertical layer structures. Using a semi-deterministic fitting algorithm, the gain function can be cast into a suitable mathematical form that can be used in the FDTD method, while preserving causality in the time domain. Our fitting routine yields accurate results for a large wavelength range. Similarly, we achieve high accuracy for modelling the dielectric function of the metal grating used in the validation of the algorithm.

The hardware limitations are overcome by using a non-uniform meshing algorithm, yielding higher mesh densities for areas with small geometrical features. A new interpolation method is used in order to reduce spurious reflections from mesh boundaries. The algorithm is also developed for use on parallel computers making it possible to fit large structures into distributed memory.

We validate our algorithm by simulating different photonic crystal laser structures. We consider a PC membrane laser, a high-Q cavity laser and a polymer laser based on a metallic nano-particle grating.

Extended Maxwell's equations and FDTD formulation

For an adequate representation of the material gain we need to consider both the frequency dependent behaviour of the lasing material and fluctuations of the carrier density due to spatial hole burning and carrier depletion. As shown by [6], the material gain can be linked to a frequency dependent conductivity J_t, which we include in the standard set of Maxwell's equations as

$$\varepsilon \frac{\partial E}{\partial t} = \nabla \times H - J_t \qquad \mu \frac{\partial H}{\partial t} = -\nabla \times E \tag{1}$$

J_t can be a single Lorentzian or as in this paper a sum of N individual Lorentzian poles. By using a multipole formulation the fit to the material gain yields much more accurate results than alternative formulations [7]. Each single Lorentzian pole yields a second order differential equation in the time domain as

$$T_k^2 \frac{\partial^2 J_k}{\partial t^2} + 2T_k \frac{\partial J_k}{\partial t} + (1+\omega_k^2 T_k^2) J_k = \frac{\sigma_k}{1+I/I_S}\left(E + T_k \frac{\partial E}{\partial t}\right) \tag{2}$$

where I denotes the optical intensity and I_S the saturation intensity. The coefficients T_k, ω_k and σ_k for each pole are dependent on the carrier density and denote the relaxation time, the resonant frequency and the peak gain, respectively. The non-linear dependence of the gain saturation on the optical intensity, which is determined by the spectral hole-burning and/or hot carrier effects, is included in our gain model by the factor $(1+I/I_S)^{-1}$. As given by [8] the carrier density is linked to the electric field and the current density as

$$\frac{\partial N}{\partial t} = \frac{2}{\hbar\omega_0} E \sum_{k=1}^{N} J_k - \frac{N}{\tau} + W_P \tag{3}$$

where τ is the carrier lifetime, ω_0 is the frequency of the gain peak and W_P the electrical pump rate. The above equations provide the complete updating scheme that is discretized using centred finite differences in both space and time as shown by [4]. It is, however, important to make sure that fields on the left- and right-hand side of the equations are centred on equivalent time-steps, as failing to do so leads to numerical instability [7]. We therefore apply a semi-implicit discretization scheme, which is solved to yield explicit updating equations for all fields.

Semideterministic fitting routine

In order to include the material gain in our algorithm, we need to obtain the Lorentzian parameters in equation 2 as a function of carrier density. The fitting routine therefore needs to obtain a set of parameters for each of the material gain sets. We use the commercial product Harold [5] to obtain material gain data for our quantum-well gain structure. The fitting routine is performed before the actual FDTD algorithm is started. It is important to control the fitting routine such that the fitted parameters vary smoothly with increasing carrier density. Therefore we apply a semi-deterministic fitting routine as shown schematically in figure 1, using an adaptive non-linear least-squares algorithm as described in detail in [9]. We fit each individual gain curve with a set of four Lorentzians. Each pole corresponds to a determined

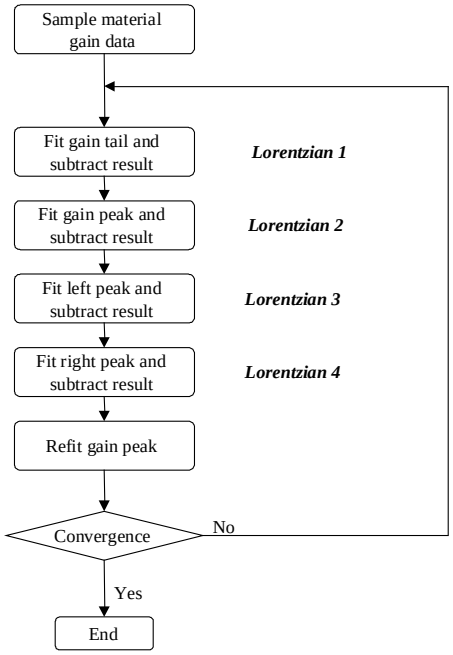

Fig. 1: Flow chart for the fitting routine for gain materials.

spectral position in order to fit the gain peak, curvature and absorption in the vicinity of the peak with high accuracy. We fit one pole at a time and then subsequently subtract the fitted result from the original data. This way dominant resonance peaks in the gain spectrum are individually removed. We first fit the absorption tail of the gain curve, followed by the gain peak. Subsequently spurious resonances to the left and right of the peak are removed with one additional pole each. Because the sum of these four Lorentzians might not represent the peak gain well, we refit the gain peak. This cycle of fitting can be applied repeatedly. We find that the algorithm converges very quickly to the local optimum in only one or two iterations. Representative results from our algorithm are shown in figure 2. As required, the fitting algorithm yields a close match to the gain

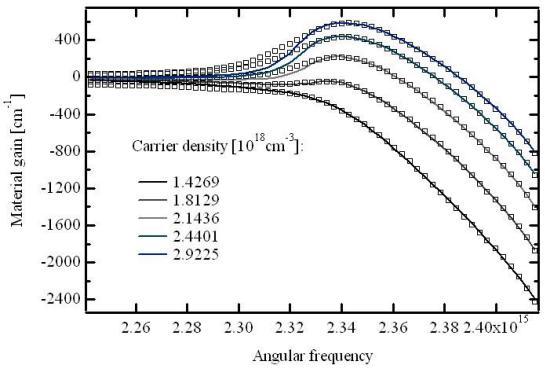

Fig. 2: Fitted gain curves for varying carrier density. Each fit is composed of four Lorentzian resonances that preserve gain peak and curvature as well as long-wavelength absorption.

peak, curvature and long-wavelength absorption tail. We note that a better fit to the left side of the peak could be obtained by selecting a greater number of poles. However, this increases the computational burden of the FDTD algorithm and also worsens the trajectory of the Lorentzian parameters. In figure 3 we show the trajectories for the peak Lorentzian as a function of carrier density. In order to facilitate evaluation in the FDTD updating scheme, we approximate the trajectory with a polynomial, fitted

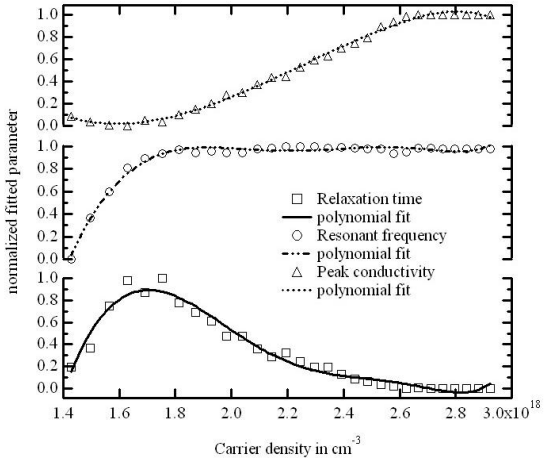

Fig. 3: The trajectory of the parameters of the peak Lorentzian with varying carrier density. Shown is also a polynomial fit of fifth order.

also in a least-squares sense. Because the parameters vary without major jumps, a polynomial of fifth order is sufficient to represent the trajectory. Polynomials can be evaluated at minimal costs and are therefore ideally suited for a fast FDTD algorithm.

Mesh refinement and distributed computing

As suggested by [4], the FDTD algorithm requires a spatial resolution of roughly 20 grid points per wavelength in order to yield a numerical accuracy of 1 %. Because this criterion is dependent on the refractive index of individual geometrical features, small shapes with high refractive index impose an unnecessary stringent grid resolution for the computational domain. We therefore implement a mesh refinement scheme, which provides higher resolution

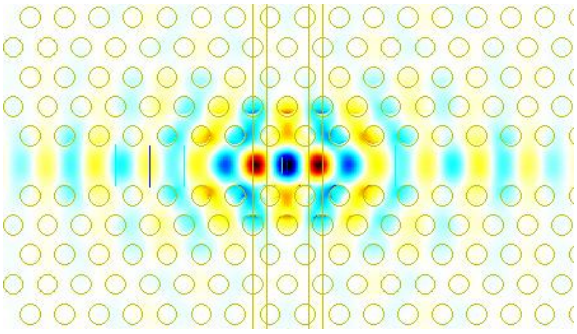

Fig. 4: Lasing mode at steady state for the high Q laser.

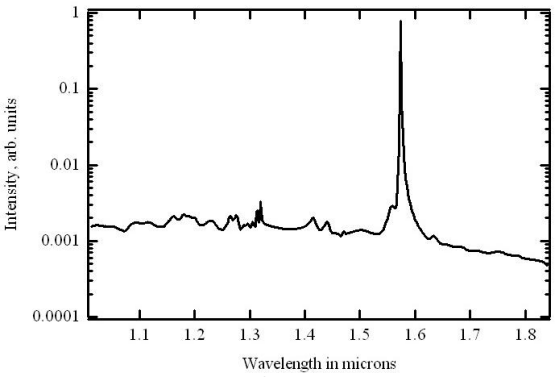

Fig. 5: Spectral response of the nano-cavity laser. The lasing peak is positioned at the resonance frequency of the cavity at 1.574 microns.

in areas with high refractive index, such as metallic particles. We choose a refinement factor of two. This refinement scheme can however by recursively applied to yield smaller grid steps. A factor of two is chosen because higher refinement steps yield higher reflections from refinement boundaries. A further reduction in reflection can be obtained by using a parabolic interpolation scheme in order to obtain boundary points for the refined region.

Though the use of non-uniform meshes reduces memory requirements significantly, three-dimensional problems still challenge computational hardware. Because many research facilities do not have access to supercomputing equipment, it is convenient to use in-house cluster systems formed by linking personal computers to a distributed environment. We split the computational domain into regions that fit into the memory of each machine. An mpi-based message passing system is employed to make sure that neighbouring domains have access to required information. The distributed version of the software not only allows us to reduce calculation time, but more importantly increases the size of problems that can be treated by the FDTD.

Numerical experiments

In order to evaluate the proposed algorithm we numerically investigate several photonic crystal laser geometries.

Ultra-high Q cavity laser

In a first example we compute the lasing spectrum for a nano-cavity membrane laser. The nano-cavity is designed as described by [10]. Nano-cavity lasers have attracted interest in recent years due to low threshold and fast tuning speeds. The ultra-high Q cavity provides a nice way to realize a laser, because the optical pumping can be provided through the waveguide channel in the photonic crystal lattice. The cavity is composed of a hetero photonic crystal lattice with lattice constants I=410 nm and lattice constant II=420 nm. The membrane thickness was set to 287 nm. This cavity design shows a resonance peak at 1.574 microns. The high quality factor of the cavity results from the dual lattice nature of the structure. Wavelengths are allowed in the region with larger lattice constant that cannot propagate in the regions with smaller lattice constant. When the waveguide in photonic crystal II is short enough, the frequencies that photons are allowed in this region become quantized - similar to the situation for electrons in a semiconductor quantum structure. We apply our algorithm to this particular structure. We choose a grid spacing of 25 nm and propagate the fields for 5 ps to ensure that the laser has reached steady state. The lasing output is recorded in the air space above the membrane. In figure 4 we show the

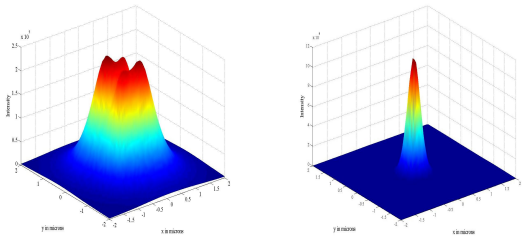

a) **b)**

Fig. 6 a) Far field obtained for a single defect cavity. **b)** Far field for 7 coupled nanocavities.

lasing mode once the laser has reached steady state. The cavity mode is clearly visible for the resonant frequency of 190.5 THz. The spectral response of the laser reveals a central peak at 1.574 microns as shown in figure 5.

Nano-cavity array membrane laser

In a second example we consider the beam characteristics of coupled nano-cavity lasers. Such membrane laser arrays have can provide ultra-fast modulation speeds [3]. Here we consider a thin membrane of 280 nm thickness. A hexagonal photonic lattice with lattice constant 365 nm is inscribed into the membrane, where the hole diameter is set to 175 nm. InP is chosen as a material system with 4 quantum wells included in the membrane to yield a peak gain around 1.25 microns. Cavities are generated in the membrane by removing a single hole from the lattice. Choosing only one defect atom allows us to preserve the symmetry of the lattice and therefore obtain better mode shaping properties. In this experiment we study the far field behaviour of single and coupled cavities. As shown

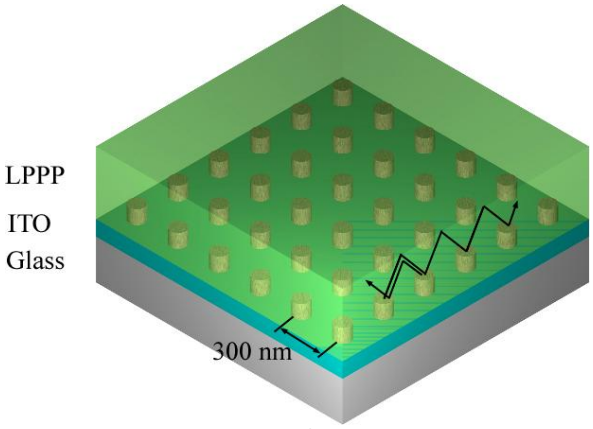

Fig. 7: Geometrical structure of the polymer PC laser. Optical feedback is provided through second-order Bragg scattering as indicated by the black arrows.

in figure 6a), a single cavity does not result in a directional output beam. However, by coupling 7 cavities a supermode exists in the photonic crystal lattice that does yield a directional output, as demonstrated in figure 6b). Furthermore, the output intensity is increased by a factor of approximately 4.8. The simulation confirms therefore the possibility to improve the output characteristics of coupled cavity lasers with numerical techniques.

Polymer laser with a metallic nano-particle grating

In the last numerical example we investigate lasing behaviour in a polymer laser. Since the demonstration of stimulated emission in organic semiconductors this field of research has attracted increasing interest. In this study we employ the optical feedback mechanism described by Stehr et al. [2] consisting of a grating of gold nano-discs. The simulated structure is shown in figure 7. A 110 nm thin layer of indium tin oxide (ITO) on a glass substrate is used as the substrate for the metal grating. The gold discs of diameter 110 nm and 30 nm height form a two-dimensional photonic crystal lattice with a lattice constant of 300 nm. The grating provides feedback through second order Bragg scattering. A thin methyl-substituted ladder-type poly(para phylene) (LPPP) layer of 460 nm thickness is chosen as a gain medium with an emission peak at 490 nm. We consider six rows of photonic crystals in this investigation. The global grid resolution is set to 20 nm. In order to achieve high accuracy for the metal disks, we enclose them in a subgridding region of refinement factor 4, meaning that we use a mesh density that is four times higher than in the global grid. The computational domain is terminated with uniaxial perfectly matched layers in order to absorb reflections from the grating structure. The total simulation time is set to 5 pico-seconds and the lasing output is recorded above the LPPP layer in air. In figure 8 we show the spectral response of the polymer laser. A clear peak is visible at 476 nm in the blue visible range. This peak corresponds to the Bragg wavelength of the grating in second order mode. The lasing output is coupled out of the LPPP layer

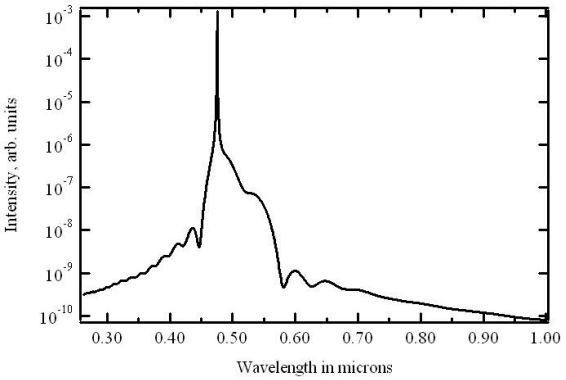

Fig. 8: Spectral response of the polymer PC laser.

through the first order mode as shown in [2].

Conclusions

We have presented a novel flexible FDTD algorithm that is capable of simulating lasing in complex material systems in three dimensions. We fit the gain material to a multi-pole Lorentzian model using a semi-deterministic fitting algorithm providing accuracy over a wide spectrum. Saturation effects and spatial hole burning are included through rate equations and a non-linear saturation model. The algorithm uses mesh refinement techniques and is developed for use in a distributed cluster system thus allowing for numerical investigation of large devices. The validity of the approach was demonstrated by simulating a variety of photonic crystal laser structures. We investigated lasing in nano-cavity membrane lasers and polymer based lasers with a gold nano-particle grating.

Acknowledgements

Wolfram H.P. Pernice would like to thank Photon Design for funding a DPhil. Research studentship.

References

1 N. Yokouchi et al., IEEE Sel.Top. Quantum Electr., vol. 9, no. 5, pp. 1439-1445, 2003.
2 J. Stehr et al., Advanced Materials, vol. 15, p. 1726, 2003.
3 H. Altuc et al., Nature Physics, vol. 2, pp. 484-489, 2006.
4 A. Taflove and S. C. Hagness, "Computational Electrodynamics: The Finite-Difference Time-Domain Method", Boston: Artech House, 2005.
5 Harold, Photon Design, 34 Leopold Street, OX4 1TW Oxford, U.K.
6 S. C. Hagness et al., Radio Sci., vol. 31, no. 4, pp. 931-941, 1996.
7 M. Bahl et al., IEEE Journal of Quantum Electronics, vol. 41, no. 10, pp. 1244-1252, 2005.
8 A. E. Siegman, Lasers. Mills Valley, CA: Univ. Sci. Books, 1986.
9 J. E. Dennis et al., ACM Trans. Math. Softw, vol. 7, no. 3, pp. 348-368, Sept. 1981.
10 B-S. Song et al., Nature Materials, vol. 4, pp. 2007-2010, 2005.